



Development of polystyrene based nanoparticles ions exchange resin for water purification applications

M.S. Mohy Eldin^{a,b,*}, M.A. Abu-Saied^b, T.M. Tamer^b, M.E. Youssef^c, A.I. Hashem^b, M.M. Sabet^b

^aFaculty of Science, Chemistry Department, University of Jeddah, Osfan, P.O. Box 80203, Jeddah 21589, Saudi Arabia, Tel. +203 4593 414; email: m.mohyeldin@mucsat.sci.eg

^bPolymer Materials Research Department, Advanced Technology and New Materials Research Institute, MuCSAT, New Borg El-Arab City 21934, Alexandria, Egypt, Tel. +203 4593 414; emails: mouhamedabdelrehem@yahoo.com (M.A. Abu-Saied), ttamer85@yahoo.com (T.M. Tamer), Tel. +201 05758908; email: aihashem@yahoo.com (A.I. Hashem), Tel. +203 4593 414; email: maysamohamed19@yahoo.com (M.M. Sabet)

^cComputer-Based Engineering Applications Department, Informatics Research Institute, MuCSAT, New Borg El-Arab City 21934, Alexandria, Egypt, Tel. +203 4593 410; email: elsayed168@yahoo.com

Received 24 January 2015; Accepted 24 June 2015

ABSTRACT

A poly(styrene-co-4-vinylbenzenesulfonic acid) copolymer nanoparticle ion exchanger has been developed using a precipitation polymerization technique. The factors that affect the polymerization process, including the polymerization time, polymerization temperature, initiator concentration, solvent polarity, and comonomer composition, were studied. The copolymer particle size and its ion-exchange capacity were controlled by varying the conditions of the polymerization process. The copolymer structure was investigated using FT-IR and TGA analyses. In addition, the particle size and morphology were investigated using a particle size analyzer and SEM, respectively. Finally, the developed ion-exchange nanoparticles were applied for water purification and the ion-exchange process was modeled.

Keywords: Precipitation polymerization; Copolymers; Nanoparticles; Styrene; 4-vinylbenzene

1. Introduction

Copolymer nanoparticles are an important class of copolymer material that has been utilized in a wide range of applications, including solid-phase synthesis, chromatography [1], controlled release systems [2,3], molecular imprinting technology [4–6], and water purification. This material is also a candidate for use in information technology, electrical and electronic

applications, and biotechnology [7,8]. The preparation of micron- or nanosized polymer spheres that have monodispersed, highly cross-linked and stable structures using conventional methods, such as suspension, dispersion, or emulsion polymerization techniques, is challenging. Precipitation polymerization is a novel and attractive method for preparing highly cross-linked, monodispersed polymer microspheres with a narrow particle size distribution and more homogeneous binding sites in the absence of a surfactant or stabilizer [9,10].

*Corresponding author.

In a precipitation polymerization process, the polymerization occurs in a solvent medium that solvates the functional monomer, template molecule, cross-linker and initiators but not the obtained polymer. The polymer particles are not stabilized and tend to agglomerate and precipitate from the solvent to form particles with a narrow size distribution. In this process, no emulsifier or suspending reagent is added. Therefore, the copolymer is highly pure [11]. Copolymer particles with a narrow particle size distribution and more homogeneous binding sites can be obtained using this method [12,13]. The use of a copolymer resin for water purification is well known since the early twentieth century, where an ion-exchange resin is used to remove unfavorable ions such as heavy metals and hard ions. Aniceto et al. modeled the ion-exchange equilibrium in the analysis of exchanger-phase non-ideality. In their study, the performance of the NRTL, Margules, and UNIQUAC models was compared with that reported by Wilson to evaluate their applicability to the area of ion-exchange equilibrium [14]. Aniceto et al. later also modeled the ion-exchange equilibrium of ternary systems using neural networks, and their results indicated that artificial neural networks (ANNs) are highly advantageous [15]. We have synthesized different nanopolymer and nanocopolymer particles using the precipitation polymerization technique for various applications, including heavy metal removal [16,17], dye removal [18,19], and enzyme immobilization [20,21].

In the current work, a poly(styrene-co-4-vinylbenzenesulfonic acid) copolymer nanoparticle ion exchanger was developed using the precipitation polymerization technique to prepare particles with a narrow size distribution from two monomers (i.e. styrene and 4-vinylbenzenesulfonic acid sodium salt). The polymerization process was studied by estimating the copolymer yield and the particle sizes of the generated copolymer nanoparticles. In addition, the ion-exchange capacity (IEC) of the copolymer nanoparticles was determined and further tested for the removal of water hardness.

2. Materials and methods

2.1. Materials

Ethanol (purity 99.9%), methanol (purity 99.8%), acetone (purity 99.5%), 1-propanol (purity 99.8%), and 2-propanol (purity 99.8%) were obtained from International Co. for Supp. & Med. Industries (Egypt). 4-Vinylbenzenesulfonic acid sodium salt (Sst; purity 99%, Mw 206.20) was obtained from Fluka (Switzerland). Styrene (St; purity 99%, Mw 104) and potassium persulfate

(KPS; purity 99%, Mw 270.31) were obtained from Sigma–Aldrich Chemicals (Germany).

2.2. Preparation of copolymer nanoparticles

The copolymer nanoparticles were prepared using a precipitation polymerization technique. Different monomer molar ratios (i.e. St:Sst ratios of 90:10, 70:30, 50:50, 30:70, and 10:90) were used. A KPS initiator solution in ethanol/water (0.37–3.7 mmol) was used to dissolve the comonomers. The solution was mixed and left to stand for 4 h at 60°C in a water bath. The solution changed to a milky state, which indicated the formation of the copolymer nanoparticles. The samples were maintained at RT for 24 h to allow the post-polymerization process to proceed and were subsequently centrifuged at 20,000 rpm to separate the suspended copolymer particles from the polymerization medium. The copolymers were then washed three times to remove the unreacted monomers and initiator residues. The copolymers were subsequently dried at 80°C for 24 h prior to being weighed to calculate the copolymer yield [19].

2.3. Preparation of alginate-encapsulated copolymer nanoparticles

Five hundred milligrams of the copolymer nanoparticles was dispersed in 25 mL of distilled water and mixed well with the alginate solution (2 g dissolved in 50 mL of distilled water). The resulting viscous composite solution was ionically cross-linked by dropwise addition to a 0.1 M CaCl₂ solution, shaken overnight and then filtered. The filtrate was complexometrically titrated to determine the residual Ca²⁺ ions. Alginate blank samples that did not contain copolymers were prepared, and the amount of Ca²⁺ ions consumed in the cross-linking process was subtracted from that consumed in the cross-linking of the copolymer–alginate samples to determine the exact amount of Ca²⁺ ions exchanged by the copolymer nanoparticles.

2.4. Ca²⁺ ion determination by complexometric titration

2.4.1. Preparation of 0.1 M EDTA solution

Approximately 20 g of EDTA dihydrate (Na₂H₂Y₂·2H₂O) was dried in an oven at 80°C for 1 h. A 9.5 g sample of EDTA was weighed and transferred to a 250-mL volumetric flask. The contents of the flask were dissolved in distilled water and then diluted to the mark.

2.4.2. Preparation of buffer solution (pH 10)

Ninety grams of ammonium chloride was dissolved in 375 mL of 28–30% ammonium hydroxide and diluted to 500 mL with water (the pH of a 1 + 10 dilution with water should be approximately 10).

2.4.3. Titration of Ca^{2+} ions

The filtrate from the previous experiment was transferred to a 250-mL Erlenmeyer flask. Eriochrome Black T indicator and 10 mL of the buffer solution (pH 10) were added to each sample. The solution was titrated with a standardized EDTA solution.

2.5. Determination of water hardness using a flame photometer

A Beckman quartz spectrophotometer with a flame attachment was used. The light from the flame was measured on the transmission scale of the instrument because the units on this scale are linearly related to the intensity of the light. The settings of the instrument are somewhat arbitrary, and the following settings serve only as a guide. The calibration curves may vary slightly with different settings and different instruments and should be verified for each instrument. The reading on the transmission scale was recorded for distilled water and four different standard solutions to determine the standard curve shown in Fig. 1.

2.6. Copolymer characterization

2.6.1. Turbidity measurements

The optical density of the dilute aqueous copolymer solutions was monitored at 500 nm using an

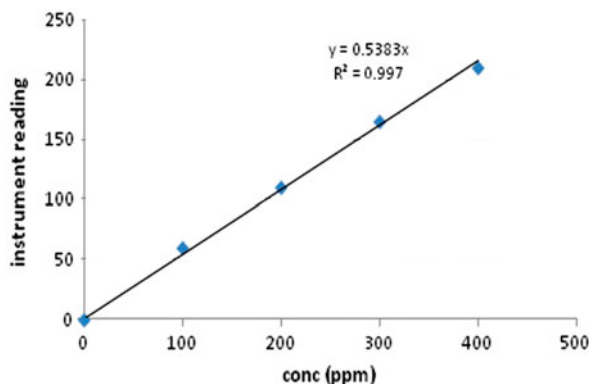


Fig. 1. Standard curve for Ca^{2+} ions by flame photometry.

Ultrospec spectrophotometer. For the turbidimetric studies, the measurements were performed at different concentrations ranging from 0.005 to 0.1 g/10 mL.

2.6.2. Infrared spectroscopic analysis

The copolymer functional groups were investigated using a Fourier transform infrared spectrophotometer (Shimadzu FTIR-8400 S, Japan) connected to a PC, and the analysis of the data was accomplished using the IR Solution software, version 1.21.

2.6.3. Thermogravimetric analysis

Thermogravimetric analysis (TGA) of the copolymer nanoparticles was carried out using a thermogravimetric analyzer (Shimadzu TGA-50, Japan); the samples were heated at 10°C/min in the temperature range from 20 to 600°C under nitrogen flowing at 20 mL/min.

2.6.4. Scanning electron microscopy

The scanning electron microscopy (SEM) images of the copolymer particles were collected using a scanning electron microscope (JEOL JSM 6360LA, Japan) at an accelerating voltage of 20 kV. The particles were affixed to carbon tape attached to aluminum SEM stubs and coated with gold to a thickness of a few nanometers under vacuum.

2.7. Mathematical model of the ion-exchange process

The governing equation that describes the ion-exchange resin is derived from the Nernst–Planck equations for two ion species A and B. The porous structure of the resin is neglected, and the resin is treated as a quasi-homogeneous phase. The concentrations of the ion groups are assumed to be constant. Under these assumptions, the ion species fluxes A and B are given by the Nernst–Planck equations shown in Eqs. (1) and (2), respectively. A spherical coordinate system is used in 1-D under spherical symmetry to derive the dimensionless form shown in Eq. (3) from Eqs. (1) and (2):

$$\Phi_A = -D_A \left[\text{grad } C_A + Z_A C_A \left(\frac{\mathcal{F}}{RT} \right) \text{grad } \varphi \right] \quad (1)$$

$$\Phi_B = -D_B \left[\text{grad } C_B + Z_B C_B \left(\frac{\mathcal{F}}{RT} \right) \text{grad } \varphi \right] \quad (2)$$

$$\frac{\partial \gamma}{\partial \tau} - \frac{1}{\rho^2} \frac{\partial}{\partial \rho} \left[\frac{1 + b\gamma}{1 + a\gamma} \rho^2 \frac{\partial \gamma}{\partial \rho} \right] = 0 \quad (3)$$

$$\gamma = \frac{Z_A C_A}{C} \quad \tau = \frac{D_A t}{r_o^2} \quad \rho = \frac{r}{r_o} \quad (4)$$

where Φ is the flux, D is the individual diffusion constant, \mathcal{F} is the Faraday constant, R is the gas constant, T is the absolute temperature, ϕ is the electric potential, C_i is the molar concentration of species i , Z_i is the valence of species i , r is the radial spherical coordinate, and r_o is the bead radius. The finite difference method has been used to discretize Eq. (3) as follows:

$$\begin{aligned} \gamma(\rho, \tau + \Delta\tau) = & \gamma(\rho, \tau) + \frac{\Delta\tau}{\Delta\rho^2} \{ R_+ D_+ [\gamma(\rho + \Delta\rho, \tau) \\ & - \gamma(\rho, \tau)] - R_- D_- [\gamma(\rho, \tau) - \gamma(\rho - \Delta\rho, \tau)] \} \end{aligned} \quad (5)$$

$$R_+(\rho) = \left[\frac{\rho + \frac{1}{2}\Delta\rho}{\rho} \right]^2 \quad (6)$$

$$R_-(\rho) = \left[\frac{\rho - \frac{1}{2}\Delta\rho}{\rho} \right]^2 \quad (7)$$

$$D_+(\gamma) = \frac{2 + b[\gamma(\rho + \Delta\rho, \tau) + \gamma(\rho, \tau)]}{2 + a[\gamma(\rho + \Delta\rho, \tau) + \gamma(\rho, \tau)]} \quad (8)$$

$$D_-(\gamma) = \frac{2 + b[\gamma(\rho, \tau) + \gamma(\rho - \Delta\rho, \tau)]}{2 + a[\gamma(\rho, \tau) + \gamma(\rho - \Delta\rho, \tau)]} \quad (9)$$

where a and b are constants

$$a = \frac{Z_A D_A}{Z_B D_B} - 1 \quad \text{and} \quad b = \frac{Z_A}{Z_B} - 1 \quad (10)$$

$$-\frac{dQ_A}{dt} = -\frac{VCD_A}{r_o^2} \frac{dq_A}{d\tau} \quad (11)$$

$$q_A(\tau) = 3 \int_0^1 \gamma(\rho, \tau) \rho^2 d\rho \quad (12)$$

where Q_A is the amount of species A in the bead and V is the bead volume. According to Simpson's rule,

$$q_A(\tau) = (\Delta\rho)^3 \left[4 \sum_{n=1,3,5}^{\frac{1}{\Delta\rho}-1} n^2 \gamma(\rho, \tau) + 2 \sum_{n=2,4,6}^{\frac{1}{\Delta\rho}-2} n^2 \gamma(\rho, \tau) \right] \quad (13)$$

where

$$n = \frac{\rho}{\Delta\rho} \quad (14)$$

$$F(\tau) = 1 - q_A(\tau) \quad (15)$$

where $F(\tau)$ represents equilibrium fractional attainment.

To solve Eq. (2), initial and boundary conditions are applied as follows:

$$\gamma(\rho, \tau = 0) = 1 \quad 0 \leq \rho < 1 \quad (16)$$

$$\gamma(\rho = 1, \tau) = 0 \quad \text{and} \quad \gamma(\rho = 0, \tau) = \gamma(\rho = \Delta\rho, \tau) \quad (17)$$

The stability condition for the discretized equation is

$$\Delta\tau = 0.4 \frac{\Delta\rho^2}{D_{\max}} \quad (18)$$

$$D_{\max} = 1 \quad \text{if} \quad a > 0, \quad b < 0 \quad (19)$$

$$D_{\max} = \frac{1 + b}{1 + a} \quad \text{if} \quad a < 0, \quad b > 0 \quad (20)$$

3. Results and discussion

A poly(styrene-co-4-vinylbenzenesulfonic acid) copolymer nanoparticle ion exchanger was developed using the precipitation polymerization technique, as shown in Fig. 2. To optimize the characteristics of the resulting copolymers, the various parameters that control the polymerization process (i.e. the comonomers' composition, comonomer and initiator concentrations, polymerization time, polymerization temperature, and the solvent composition) were studied. The obtained results are discussed below.

3.1. Effect of the comonomer composition

Precipitation polymerization is a modified solution polymerization technique in which the polymerization

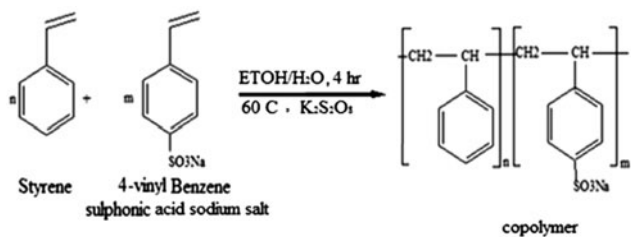


Fig. 2. Reaction between styrene and 4-vinylbenzenesulfonic acid sodium salt.

is conducted in a non-solvent of the resulting polymer. Therefore, as the reaction proceeds, the forming polymer precipitates from the solution. In our reaction, the polymerization begins as a homogenous solution in which the two monomers (i.e. styrene and styrene sulfonic acid) and the initiator were dissolved in the continuous phase, which was a cosolvent consisting of ethanol and water. Table 1 shows the effect of the comonomer composition on the copolymer yield, particle size, and IEC.

On the basis of the results in Table 1, a very slight increase in the copolymer yield was observed as the Sst concentration in the feeding monomer solution was increased. This result may be due to the similarity of the chemical structures of both monomers, which affects their reactivity. The change in the mean particle size as the comonomer composition was varied resulted in a two-stage trend. The first stage appeared at St concentrations of 90–50% (except for the 70% concentration), where the mean particle size varied slightly from 27 to 23.5 nm. The second stage involves an exponential increase in the mean particle size as the St concentration was decreased to less than 50% in the feeding comonomer solution, and the mean particle size was 750 nm at a St:Sst ratio of 10:90. This behavior may be due to an increase in the stabilization power of the sulfonic groups with increasing sulfonic group content in the copolymer particles. The IEC measurements indicated a different behavior, where a decrease was observed as the copolymer particle size and Poly Sst content increased, except for the St:Sst (70:30) composition. A minimum value (0.339 meq/g)

was obtained at a copolymer particle size of 750 nm, which was prepared using an St:Sst ratio of 10:90. Although increasing the Sst molar ratio in the comonomer composition is expected to increase the IEC, the associated increase in the particle size leads to a reduction of the exposed surface area; consequently, the number of ion-exchange sites exposed to the solution phase is reduced. A compromise between the opposing effects of the Poly Sst content of the particles and their surface area provided the obtained results.

To investigate the effect of varying the comonomer feed on the copolymer composition, the solubility in water was studied; the results from the turbidity measurements are listed in Table 2. The water solubility of the copolymer increased as the Sst content in the comonomer feeding solution increased, which may be due to enhanced coagulation of the samples lowering the optical density as the styrene molar ratio increased. In contrast, an increase in the molar ratio of styrene sulfonic acid promotes the stability of the copolymer nanoparticles due to an increase in the total surface charge. In general, all of the samples exhibit high turbidity values, especially at higher concentrations, except copolymers rich in Sst (70–90%), which are soluble under any condition.

3.2. Effect of the initiator concentration

The effect of varying the initiator concentration on the copolymer yield, particle size, and IEC for two comonomer compositions (i.e. St:Sst; 70:30 and 50:50) was studied; the obtained results are shown in Fig. 3.

Table 1
Effect of the comonomer composition on the copolymer yield, particle size, and IEC

| Comonomer composition (St:Sst) | Copolymer yield (%) | Mean particle size (nm) | IEC (meq/g) |
|--------------------------------|---------------------|-------------------------|-------------|
| 90:10 | 77.92 | 26.9 | 0.380 |
| 70:30 | 78.97 | 0.9 | 0.394 |
| 50:50 | 79.95 | 23.5 | 0.438 |
| 30:70 | 81.35 | 359 | 0.378 |
| 10:90 | 82.15 | 746.1 | 0.339 |

Table 2
Effect of the comonomer composition on the solubility of the copolymer

| Copolymer solution (W/V %) | Monomer molar ratio (St:Sst) | | | | |
|----------------------------|------------------------------|-------|-------|-------|-------|
| | 10:90 | 30:70 | 50:50 | 70:30 | 90:10 |
| 0.001 | 0 | 0 | 0 | 0.065 | 0.117 |
| 0.005 | 0 | 0 | 0.007 | 0.848 | 0.8 |
| 0.01 | 0 | 0 | 0.558 | 1.996 | 1.628 |
| 0.05 | 0 | 0 | 1.141 | 2.806 | 2.69 |
| 0.1 | 0 | 0 | 1.531 | 3.068 | 2.842 |

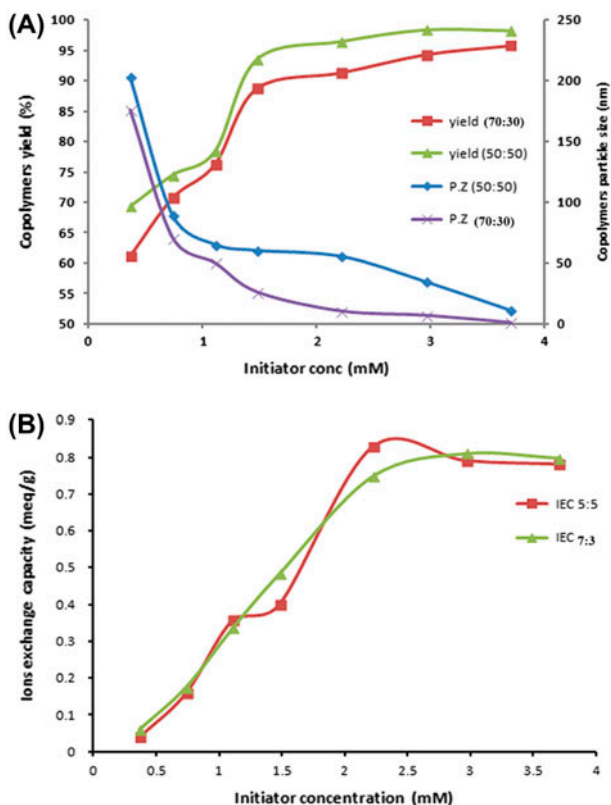


Fig. 3. Effect of the initiator concentration on (A) the copolymer yield (%) and the copolymers' particles size, and (B) the IEC (Comonomer concentration: 10%, (EtOH: H₂O 70:30), 60 °C, 4 h).

An increase in the copolymer yield was observed as the initiator concentration was increased [22]. The first part of the curve indicates a rapid increase in the conversion yield as the K₂S₂O₈ concentration was increased to 1.5 mM, where the concentration of the initiator is reaction dependent and the initiation step is the rate-determining step. The second part of the curve exhibits a slight increase in the conversion yield as the K₂S₂O₈ concentration was further increased to greater than 1.5 mM. This result is due to the limitation of the free comonomers available for polymerization because 1.5 mM KPS was sufficient to polymerize 89–93% of the two comonomer compositions with St: Sst ratios of 70:30 and 50:50, respectively.

The mean particle size of the generated copolymers was affected differently, and the curve indicates that both comonomer compositions (50:50 and 70:30) exhibit the same trend of the copolymer particle size substantially decreasing as the KPS concentration was increased to 1.5 mM, followed by reaching a plateau. This result may be due to the generation of more starting initiation seeds that share the same number of comonomer molecules, which was expected [23]. Odian

[24] argued that the kinetic chain length of radical chain polymerization is the average number of monomer molecules consumed per radical that initiated a polymer chain. The kinetic chain length was proportional to the radical concentration. Therefore, the increase in KPS concentration resulted in a lower molecular weight polymer and an increase in the number of particles per given weight of copolymer. Particles of smaller size were obtained from both studied comonomer molar ratios of 70:30 and 50:50. Ye et al. [25] argued that a higher initiator concentration would lead to grafts with a shorter oligomer chain length, resulting in increased solubility in the reaction medium. Therefore, the adsorption of the grafted stabilizer onto the particles would be retarded, which would result in the formation of larger particles. However, Song and coworkers [23] and El-Aasser et al. [26] reported that a higher initiator concentration resulted in an increased rate of generation of unstable oligomeric radicals. Because the generation rate of oligomeric radicals was much faster than the adsorption rate of the stabilizer, the oligomers tended to aggregate and form larger nuclei with various sizes before sufficient stabilizers were adsorbed to render them stable. In the current study, no stabilizer was used. However, the formed particles have a self-stabilizing sulfonic acid group that prevents aggregation. In addition, the solvent is a very poor solvent for solubilizing the copolymer particles.

The IEC curve exhibits the same trend as the copolymer yield (%), where the IEC values for the two comonomer compositions are nearly identical.

3.3. Effect of the solvent composition

Fig. 4 shows the effect of varying the cosolvent composition on the copolymer yield, particle size, and IEC. The curve indicates that the copolymer yield increased as the water content increased in the cosolvent composition. This result may be due to the increased solubility of both the Sst monomer and KPS. In the case of the ethanol enrichment media, the solubility of KPS is limited, which affects the polymerization process. This explanation is supported by the copolymer particle size results, where a decrease in the copolymer particle size was observed as the water content in the solvent was increased, which favored the formation of more initiation sites due to greater KPS solubility. The IEC curve follows the same trend as the copolymer particle size.

3.4. Effect of the polymerization time

Fig. 5 shows the effect of varying the polymerization time on the copolymer yield, particle size, and

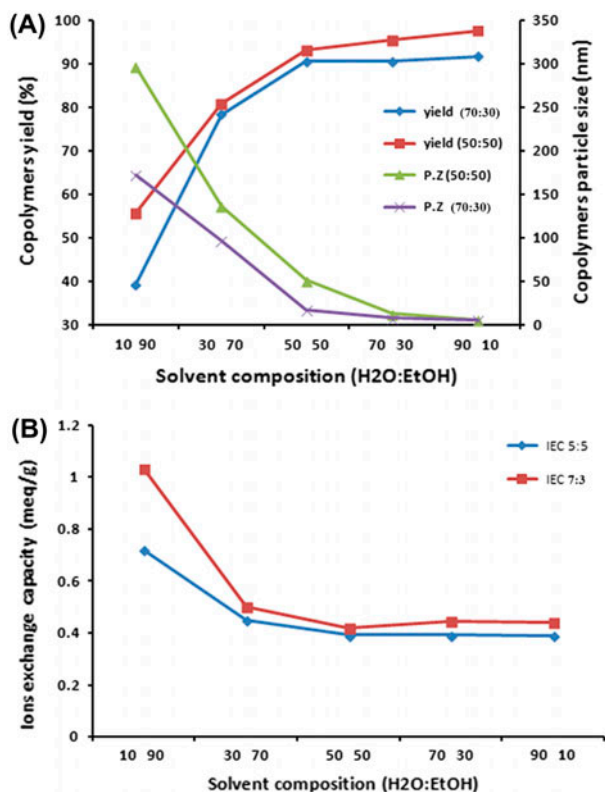


Fig. 4. Effect of the cosolvent composition on (A) the copolymer yield (%) and the copolymers' particles size, and (B) the IEC (Comonomer concentration: 10%, 1.1 mM $K_2S_2O_8$, 60°C, 4 h).

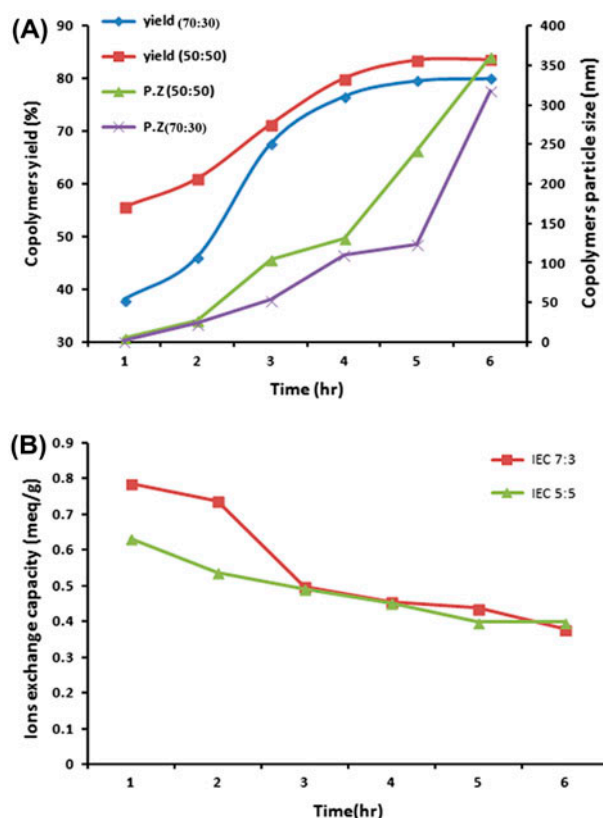
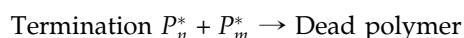


Fig. 5. Effect of the polymerization time on (A) the copolymer yield (%) and the copolymers' particles size, and (B) the IEC (Comonomer concentration: 10%, 1.1 mM $K_2S_2O_8$, (EtOH: H₂O 70:30), 60°C).

IEC. As shown in Fig. 5, an increase in the copolymer yield was observed as the polymerization time was increased from 1 to 4 h, and the copolymer yield reached a plateau until 6 h. This result may be due to the polymerization of nearly 80% of the comonomers after 4 h, which resulted in a decrease of the polymerization rate. The particle size curve indicates a typical increase in the particle size as the polymerization time increased, which may be due to the growth of the particles and is consistent with the polymerization yield curve. At longer polymerization times (6 h), an exponential increase in the particle size was observed, which may be due to the free-radical termination step that couples free-radical chains to form higher molecular weight polymers.



The variation in the IEC values as the polymerization time is increased has an inverse relationship with the particle size. The reduction in the surface area of the particles explains the IEC behavior.

3.5. Effect of the polymerization temperature

Fig. 6 shows the effect of varying the polymerization temperature on the copolymer yield, particle size, and IEC. As shown in Fig. 6, the polymerization rate increased as the polymerization temperature increased. An increase in the polymerization temperature accelerated the rate of the initiator decomposition to form free radicals because the rates of the reactions are exponentially temperature-dependent functions based on the Arrhenius law. In addition, the increase in the polymerization temperature increased the number of collisions between the initiator free radicals and the two monomers, which decreases the reaction energy barrier and promotes the polymerization process. At higher temperatures, the concentration of oligomer radicals in the aqueous phase and the nucleation rate increased; consequently, the total number of particles increased, which decreased the particle size. The same trend was observed by Meadows et al. in their simulation study [27]. The IEC was negatively affected by an increase in the polymerization

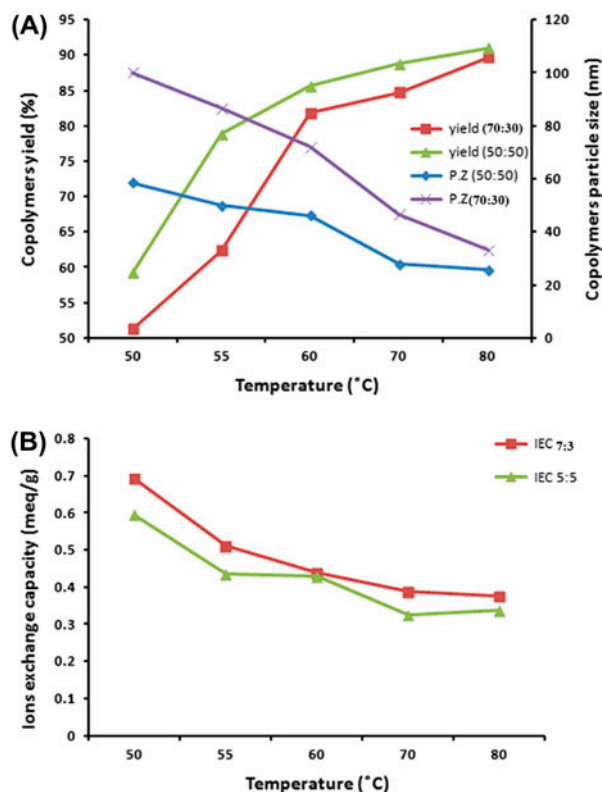


Fig. 6. Effect of the polymerization temperature on (A) the copolymer yield (%) and the copolymers' particles size, and (B) the IEC (Comonomer concentration: 10%, 1.1 mM $K_2S_2O_8$, (EtOH: H_2O 70:30, 4 h).

temperature, which is in contrast to both the copolymer yield percentage and the particle size results.

3.6. Effect of the comonomer concentration

Fig. 7 shows the effect of varying the comonomer concentration on the copolymer yield, particle size, and IEC. In general, the copolymer yield increased as the comonomer concentration was increased. The copolymer yield (%) results form a two-stage curve. The first stage exhibits a linear increase in copolymer yield from 4 to 12%, which may be due to an increase in the number of comonomer molecules available for the polymerization process because more initiation sites are available. The second stage is a plateau in the comonomer concentration range from 12 to 20%. Two factors may give rise to this behavior: the limited number of remaining comonomer molecules and the fixed number of initiator free radicals produced. However, the particle size exhibits the opposite behavior. This result may be due to the presence of an increased number of monomer molecules and a fixed amount of

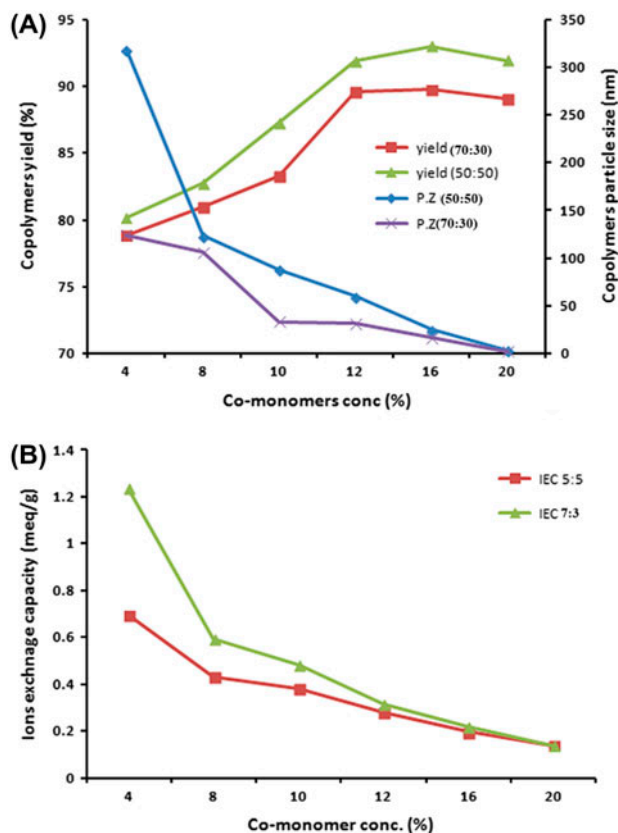


Fig. 7. Effect of the comonomer concentration on (A) the copolymer yield (%) and the copolymers' particles size, and (B) the IEC (1.1 mM $K_2S_2O_8$, (EtOH: H_2O 70:30), 60 °C, 4 h).

produced initiator free radicals in the polymerization media, which leads to an increased number of copolymer particles with a reduced size. The IEC results exhibited a similar behavior.

3.7. Effect of the solvent polarity

The polarity of the solvent plays an important role in precipitation polymerization because it must be suitable for solvation of the monomers and the initiator but unsuitable for the generated polymers. The effects on the copolymer yield, particle size, and IEC of replacing ethanol with other organic solvents with different polarities Table 3 was investigated; the results are shown in Fig. 8.

As shown in the figure, no trend was evident in the relationship between the solvent polarity and the copolymer yield. However, the number of carbon atoms of the organic solvent and the copolymer yield exhibited an inverse relationship. When the acetone results are excluded, an increase in the alcohols'

Table 3
Relative solvent polarities

| Solvent | Relative polarity |
|------------|-------------------|
| Methanol | 0.355 |
| Ethanol | 0.654 |
| Acetone | 0.762 |
| 1-Propanol | 0.617 |
| 2-Propanol | 0.546 |

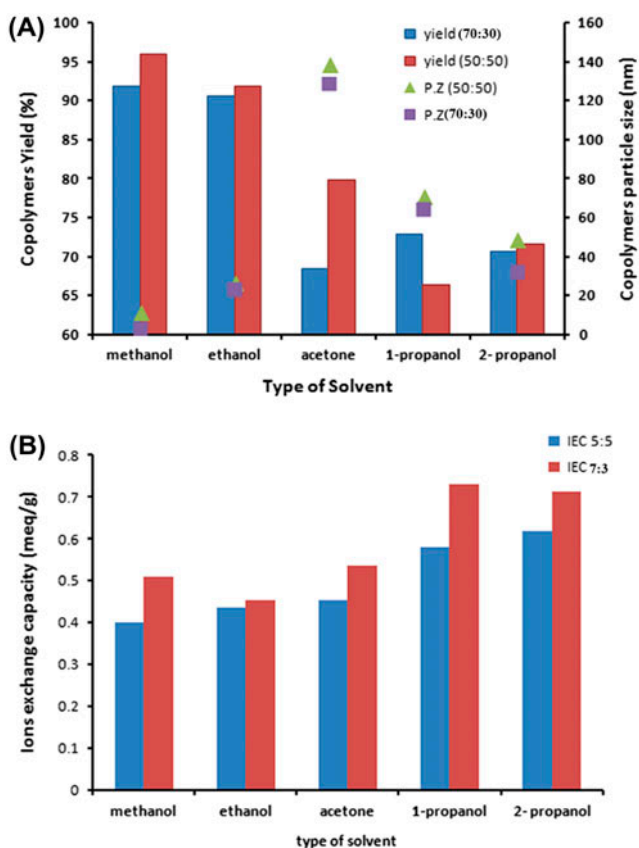


Fig. 8. Effect of the organic solvent type on (A) the copolymer yield (%) and the copolymers' particles size, and (B) the IEC (Comonomer concentration: 10%, 1.1 mM $K_2S_2O_8$, (EtOH: H_2O 70:30), 60 °C, 4 h).

polarity, which is associated with the alcohols' number of carbon atoms, led to a decrease in the copolymer yield.

In contrast, a decrease in the particle size was observed as the solvent polarity decreased. This result may be due to an acceleration of the salting-out mechanism resulting from a decrease in the stability of the copolymer in the given solvent mixture, resulting in smaller nanoparticles. The variation in the IEC

values indicates an inverse trend compared to that observed for the copolymer yield (%).

3.8. FT-IR analysis

Infrared spectroscopy is a useful qualitative tool for determining the composition of a polymer. Fig. 9 shows the spectral characteristic bands of the Poly St, Poly Sst, and Poly (St-co-Sst) polymers. The broad peak at 3,100–3,600 cm^{-1} in the spectra of all of the copolymers corresponds to –OH stretching vibrations due to the incorporation of SO_3H groups. The peaks at 2,800–3,100 cm^{-1} are attributed to various characteristic vibration bands associated with aliphatic and aromatic CH species of Poly St. In the spectrum of Poly Sst, S=O symmetric (1,041 cm^{-1}) and asymmetric stretching (1,182 cm^{-1}) bands were observed, and the sharp peak at 697 cm^{-1} corresponds to the out-of-plane bending vibration of the styrene ring. The sharp and intense peak at 756 cm^{-1} is characteristic of the out-of-plane bending vibration of the C–H groups of the monosubstituted benzene ring. The bands located at 1,620 cm^{-1} are attributed to the C=C bonds of the unreacted monomers.

3.9. Thermal characterization

TGA of the Poly (St-co-Sst) nanoparticles prepared using different comonomer molar ratios was performed. As shown in Fig. 10, the first weight loss from ambient temperature to 150 °C was due to the evaporation of adsorbed water from the sulfonic acid groups. A gradual increase in the moisture content from 4.9 to 14.7% is a direct result of the increase in the sulfonic group content in the copolymer.

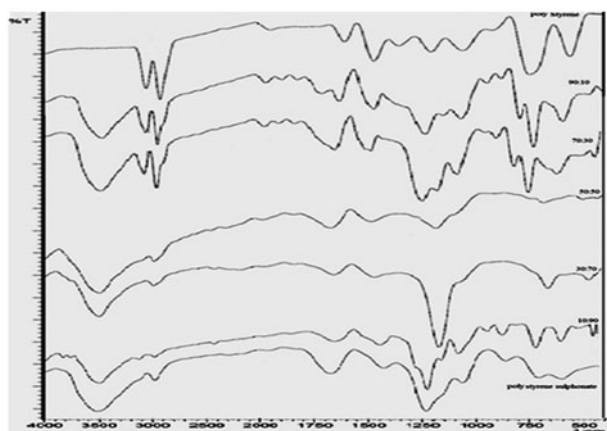


Fig. 9. FT-IR spectrum of polystyrene, poly 4-vinylbenzenesulfonic acid, and five different copolymers.

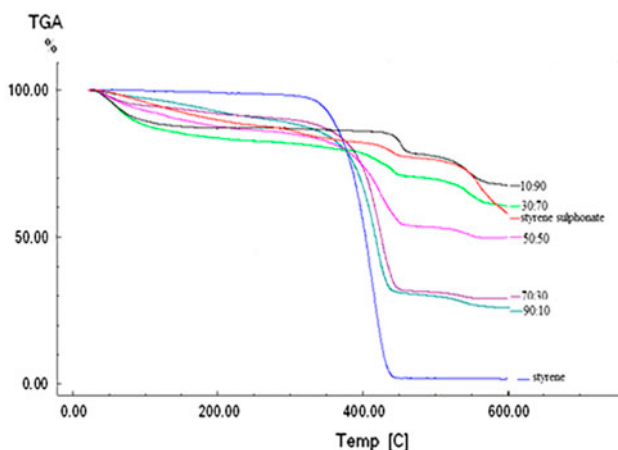


Fig. 10. TGA analysis of polystyrene, poly4-vinylstyrene-sulfonic acid, and five different copolymers.

Table 4 summarizes the thermal peaks from the TGA analysis. The depression peak at approximately 400–450 °C corresponds to styrene degradation. The results indicate an increase in the thermal stability of the copolymers as the content of the sulfonic groups increased. The next band was observed at approximately 520 °C, which was due to the degradation of the sulfonic groups. In conclusion, Table 4 shows a decrease in the weight loss percentage as the Poly Sst content in the copolymers increased.

3.10. Scanning electron microscopy

The morphological analysis of five different copolymer samples prepared using different comonomer molar ratios was performed using SEM; the results are shown in Fig. 11. On the basis of these images, a regular and homogenous distribution of the spherical nanoparticles was obtained.

3.11. Evaluation of the nanocopolymer particles for water softening

Water hardness is due to a large amount of calcium and magnesium cations in water. Hardness is typically expressed as milligrams of calcium carbonate (CaCO_3) equivalents per liter and can also be discussed in terms of carbonate (temporary) and non-carbonate (permanent) hardness. Water hardness occurs naturally in groundwater as a consequence of the weathering of limestone, sedimentary rocks, and calcium-bearing minerals. In addition, local water hardness can result from industrial effluents from chemical and mining industries or the excessive use of lime to treat the soil in agriculture fields. The hardness of water is primarily an esthetic concern because it causes an unpleasant taste and reduces the ability of soap to produce lather. In addition, water hardness causes scale formation in pipes and in distribution systems. Although the literature contains limited epidemiology studies, the published reports indicate a relationship between the hardness of water and health effects such as cardiovascular disease [28].

The removal of Ca^{2+} ions from synthetic hard water containing approximately 350 ppm of Ca^{2+} using the nanoparticle copolymers with different compositions encapsulated in alginate beads was studied. The obtained results are shown in Fig. 12. An increase in the Ca^{2+} ion removal was observed as the Poly Sst content increased. The maximum removal of 250 ppm from 350 ppm (approximately 71%) was detected at St:Sst (50:50). A further increase in the Poly Sst content led to a substantial decrease in Ca^{2+} ion removal to 41% (i.e. 143 ppm.) This behavior may be due to the substantial increase in the particle size from 23.5 nm for an St:Sst ratio of 50:50–360 and 746 nm for St:Sst ratios of 30:70 and 10:90, respectively. These changes in the particle size directly decreased the surface area of the particles, which is where the Ca^{2+} exchange process occurs.

Table 4
Thermal weight loss of Poly (St-co-Sst) nanoparticles

| St:Sst | Ambient-150 °C (%) | 150–450 °C (%) | 450–600 °C | Residue after 600 °C (%) |
|----------|--------------------|----------------|------------|--------------------------|
| Poly St | 0 | 97.5 | 0.9% | 1.6 |
| 90:10 | 4.9 | 67.2 | 5.4 | 25.74 |
| 70:30 | 6.52 | 65.47 | 3.65 | 31.13 |
| 50:50 | 10.1 | 39.17 | 5.62 | 49.61 |
| 30:70 | 12.47 | 16.59 | 12.83 | 60 |
| 10:90 | 14.7 | 11.7 | 11.27 | 67.4 |
| Poly Sst | 7.4 | 14.87 | 19.82% | 57.87 |

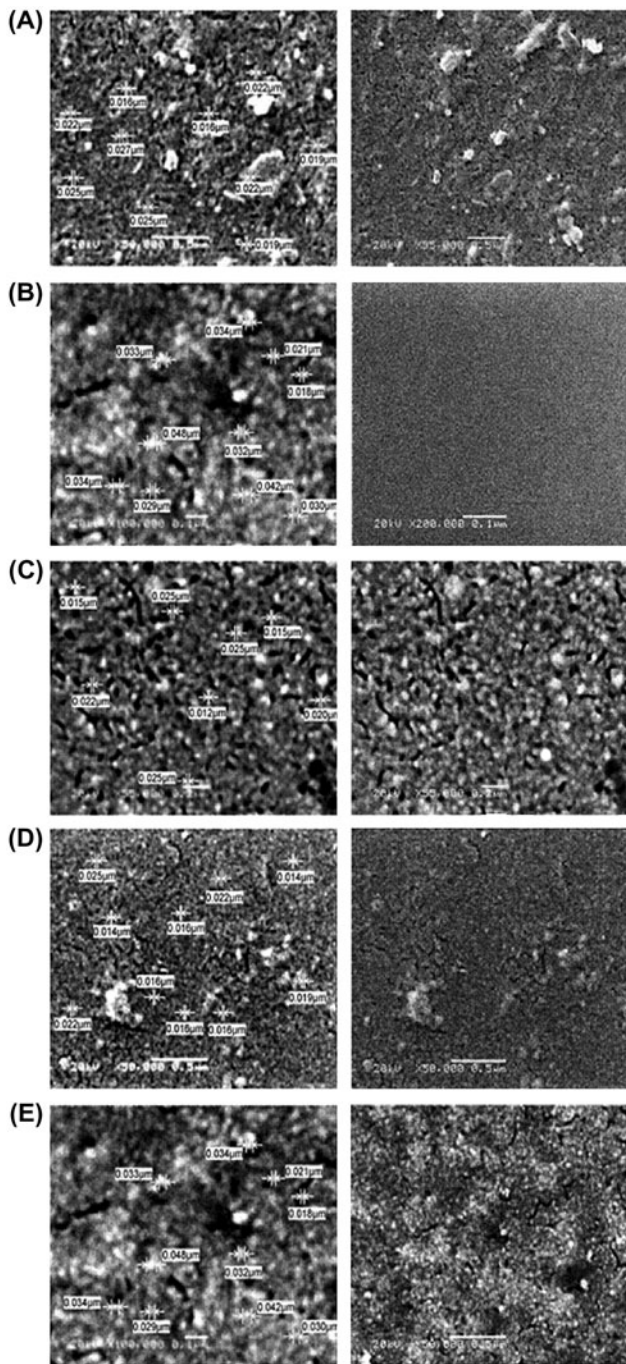


Fig. 11. SEM with different amplifications of different St: Sst molar ratio (A) 90:10, (B) 70:30, (C) 50:50, (D) 30:70, and (E) 10:90.

3.12. Calcium exchange process modeling

The dimensionless function $\gamma(\rho, \tau)$, which represents the radial concentration profiles of species A and fractional attainment of equilibrium ($F(\tau)$), was

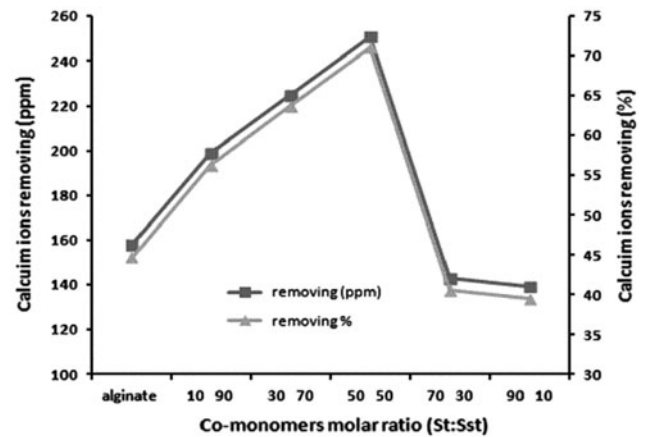


Fig. 12. Ca^{2+} ions removal from synthetic hard water treated with nanoparticles of different compositions encapsulated in alginate beads.

calculated using the previously mentioned initial and boundary conditions that depend on the diffusion constant of species A, the bead radius and the concentration. As shown in Fig. 13, the equilibrium fractional attainment $F(\tau)$ as a function of dimensionless time ($\tau = D_A t / r_0^2$), which depends on the diffusion constant of species A, was used to compare the ion-exchange processes.

Fig. 14 shows the contours of the radial concentration profiles of species A as a function of the radial coordinate and dimensionless time for both processes with different D_A/D_B ratios and different valences. The results indicate that D_A/D_B increased with $Z_A/Z_B = 1/2$ and that the ion-exchange rate decreased. However, D_A/D_B increased with $Z_A/Z_B = 2$, and the ion-exchange rate increased. An equivalent fraction of A with radial coordinates of $D_A/D_B = 20$, $Z_A/Z_B = 0.5$ and $D_A/D_B = 1/20$, $Z_A/Z_B = 2$ is shown in Fig. 15, where the equivalent fraction of A is dependent on the Z_A/Z_B ratio. Sodium ions exhibit a faster ion-exchange rate because the electric potential build up by the ion-exchange process increases the diffusion of bivalent ions and decreases the diffusion of monovalent ions.

Fig. 16 shows the fractional attainment of equilibrium for the ion-exchange process ($2\text{Na}^+(\text{resin}) + \text{Ca}^{2+}(\text{solution}) \rightarrow \text{Ca}^{2+}(\text{resin}) + 2\text{Na}^+(\text{solution})$) and reverse process ($\text{Ca}^{2+}(\text{resin}) + 2\text{Na}^+(\text{solution}) \rightarrow 2\text{Na}^+(\text{resin}) + \text{Ca}^{2+}(\text{solution})$) as a function of dimensionless time ($\tau = D_A t / r_0^2$) for ratios of 10 and 0.1 and for valences of $1/2$ and 2, respectively (ion-exchange resin); the solid line ($D_{\text{Na}}/D_{\text{Ca}} = 10$ and $Z_{\text{Na}}/Z_{\text{Ca}} = 1/2$) indicates that the exchange process was faster.

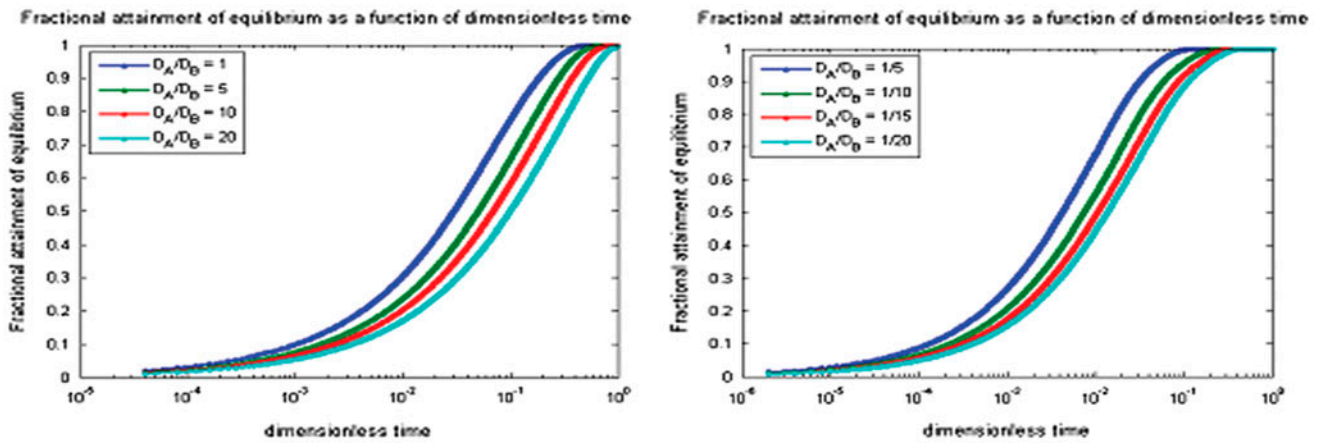


Fig. 13. Equilibrium fractional attainment as a function of dimensionless time for $Z_A/Z_B = 1/2$ (left) and $Z_A/Z_B = 2$ (right).

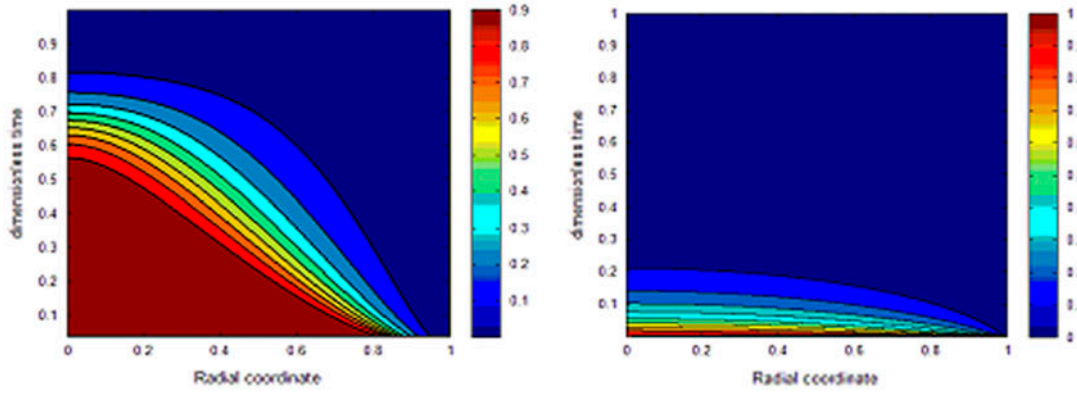


Fig. 14. Dimensionless function $\gamma(\rho, \tau)$ for $Z_A/Z_B = 1/2$ (left) and $Z_A/Z_B = 2$ (right).

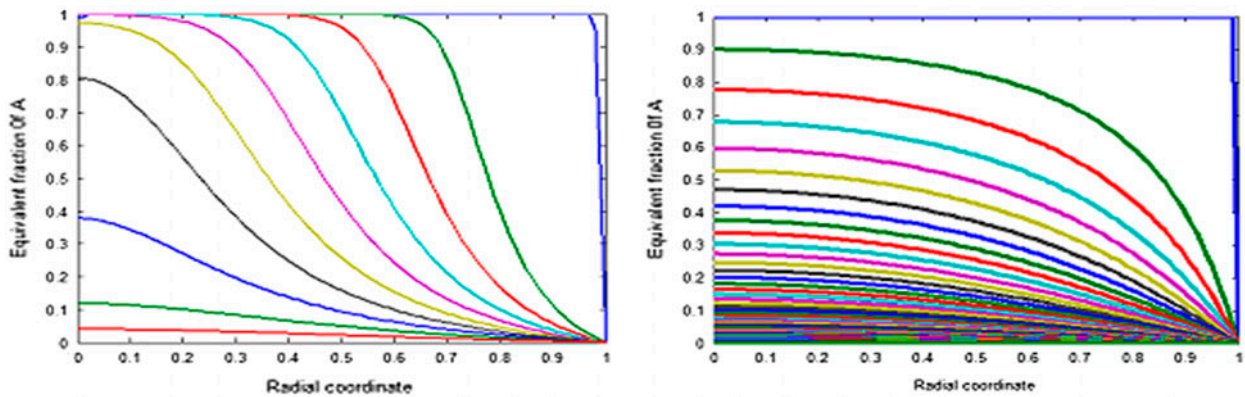


Fig. 15. Equivalent fraction of A vs. radial coordinate for $Z_A/Z_B = 1/2$ (left) and $Z_A/Z_B = 2$ (right).

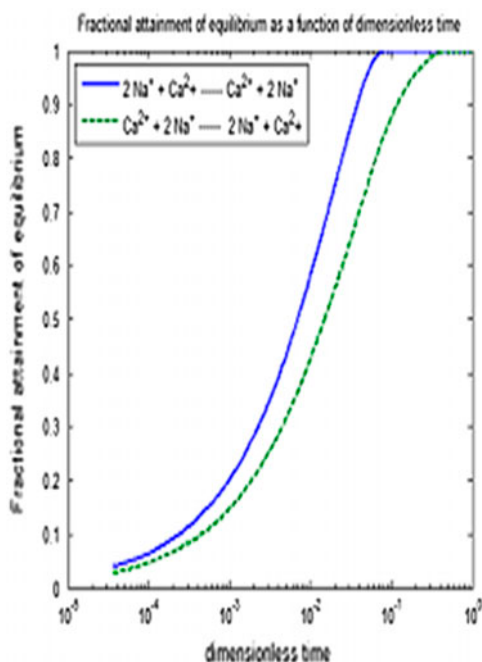


Fig. 16. $F(\tau)$ for $D_{Na}/D_{Ca} = 10$ and $Z_{Na}/Z_{Ca} = 1/2$ and $D_{Na}/D_{Ca} = 0.1$ and $Z_{Na}/Z_{Ca} = 2$, respectively, for solid and dotted line.

5. Conclusions

In this study, copolymer nanoparticles of polystyrene and poly(4-vinylbenzenesulfonic acid) were prepared via precipitation polymerization technique. The sulfonic groups on the particle enhanced the IEC, and the particles self-stabilized, which promoted the generation of nanoparticles. In this study, the polymerization process exhibited good results for an St:Sst comonomer ratio of 30:70 when acetone/water (30:70) was used as the solvent, the polymerization time was 4 h, the temperature was 70°C, and the final initiator concentration was 1.5 mM. The particle size and the IEC of the generated copolymer nanoparticles were controlled by varying the conditions of the polymerization process. The obtained particle sizes ranged from 1 to 750 nm, and the maximum IEC was obtained at 1 meq/g. The copolymer nanoparticles successfully reduced water hardness.

References

- [1] J. Haginaka, Monodispersed, molecularly imprinted polymers as affinity-based chromatography media, *J. Chromatogr. B Anal. Technol. Biomed. Life Sci.* 866 (2008) 3–13.
- [2] A. Kumari, S.K. Yadav, S.C. Yadav, Biodegradable polymeric nanoparticles based drug delivery systems, *Colloids Surf., B Biointerfaces* 75 (2010) 1–18.
- [3] J.M. Chan, P.M. Valencia, L. Zhang, R. Langer, O.C. Farokhzad, Copolymers nanoparticles for drug delivery, *Methods Mol. Biol.* 624 (2010) 163–175.
- [4] X. Kan, Q. Zhao, Z. Zhang, Z. Wang, J.J. Zhu, Molecularly imprinted polymers microsphere prepared by precipitation polymerization for hydroquinone recognition, *Talanta* 75 (2008) 22–26.
- [5] W.J. Cheong, F. Ali, J.H. Choi, J.O. Lee, K. Yune Sung, Recent applications of molecular imprinted polymers for enantio-selective recognition, *Talanta* 106 (2013) 45–59.
- [6] H. Sambe, K. Hoshina, R. Moaddel, I.W. Wainer, J. Haginaka, Uniformly sized, molecularly imprinted polymers for nicotine by precipitation polymerization, *J. Chromatogr. A* 1134 (2006) 88–94.
- [7] Y. Tunc, E. Baykara, K. Ulubayram, Fabrication of micron-sized polymer spheres by precipitation polymerization technique, *Afr. Phys. Rev. (ARP)* 84 (2008) 163–164.
- [8] S.E. Shim, S. Yang, S. Choe, Mechanism of the formation of stable microspheres by precipitation copolymerization of styrene and divinylbenzene, *J. Polym. Sci., Part A: Polym. Chem.* 42 (2004) 3967–3974.
- [9] D. Horák, Uniform polymer beads of micron size, *Acta Polym.* 47 (1996) 20–28.
- [10] K. Li, H.D.H. Stöver, Synthesis of monodisperse poly (divinylbenzene) microspheres, *J. Polym. Sci., Part A: Polym. Chem.* 31 (1993) 3257–3263.
- [11] S. Yan, Z. Gao, Y. Fang, Y. Cheng, H. Zhou, H. Wang, Characterization and quality assessment of binding properties of malachite green molecularly imprinted polymers prepared by precipitation polymerization in acetonitrile, *Dyes Pigm.* 74 (2007) 572–577.
- [12] J. Prasad Rao, E. Geckeler Kurt, Polymer nanoparticles: Preparation techniques and size-control parameters, *Prog. Polym. Sci.* 36 (2011) 887–913.
- [13] C. Vauthier, K. Bouchemal, Methods for the preparation and manufacture of copolymers nanoparticles, *Pharm. Res.* 26 (2009) 1025–1058.
- [14] J.P.S. Aniceto, S.P. Cardoso, T.L. Faria, P.F. Lito, C.M. Silva, Modeling ion exchange equilibrium: Analysis of exchanger phase non-ideality, *Desalination* 290 (2012) 43–53.
- [15] J.P.S. Aniceto, D.L.A. Fernandes, C.M. Silva, Modeling ion exchange equilibrium of ternary systems using neural networks, *Desalination* 309 (2013) 267–274.
- [16] M.S. Mohy Eldin, M.F. Elkady, M.A. Abu-Saied, A.M. Abdel Rahman, E.A. Soliman A.A. Elzatahry, M.E. Youssef, Removal of cadmium ions from synthetic aqueous solutions with a novel nanosulfonated poly (glycidyl methacrylate) cation exchanger: Kinetic and equilibrium studies, *J. Appl. Polym. Sci.* 118 (2010) 3111–3122.
- [17] M.F. Elkady, M.A. Abu-Saied, A.M. Abdel Rahman, E.A. Soliman, A.A. Elzatahry, M.E. Youssef, M.S. Mohy Eldin, Nano-sulphonated poly (glycidyl methacrylate) cations exchanger for cadmium ions removal: Effects of operating parameters, *Desalination* 279 (2011) 152–162.
- [18] M.S. Mohy, S.A. Eldin, M.M. El-Sakka, I.I. El-Masry, S.S. Abdel-Gawad, Garybe, Removal of methylene blue dye from aqueous medium by nano-polyacrylonitrile particles, *Desalin. Water Treat.* 44 (2012) 151–160.

- [19] M.S. Mohy Eldin, Y.A. Aggour, M.R. El-Aassar, G.E. Beghet, R.R. Atta, Development of nano-crosslinked polyacrylonitrile ions exchanger particles for dyes removal, *Desalin. Water Treat.* (2015), doi: [10.1080/19443994.2014.1000383](https://doi.org/10.1080/19443994.2014.1000383).
- [20] M.S. Mohy Eldin, M.R. Elaassar, A.A. Elzatahry, M.M.B. Al-Sabah, Poly (acrylonitrile-co-methyl methacrylate) nanoparticles: I. Preparation and characterization, *Arab. J. Chem.* (2014), doi: [10.1016/j.arabjc.2014.10.037](https://doi.org/10.1016/j.arabjc.2014.10.037).
- [21] M.S. Mohy Eldin, Mohamed R. Elaassar, A.A. Elzatahry, M.B. EL-Sabbah, Lactose hydrolysis using immobilized β -galactosidase enzyme onto nano-copolymers particles, *Trends Biomater. Artif. Organs* 28 (2014) 1–14.
- [22] K. Behari, L. Bahadur, R. Das, U. Agarwal, Polymerization of acrylamide by peroxodiphosphate/different activators redox system in an aqueous medium, *J. Macromol. Sci., A Pure Appl. Chem.* 31 (1994) 383–394.
- [23] B.K. Song, M.S. Cho, K.J. Yoon, D.C. Lee, Dispersion polymerization of acrylamide with quaternary ammonium cationic comonomer in aqueous solution, *J. Appl. Polym. Sci.* 87 (2003) 1101–1108.
- [24] G. Odian, *Principles of Polymerization*, Wiley, New York, NY, 1970.
- [25] Q. Ye, Z.C. Zhang, X.W. Ge, Formation of monodisperse polyacrylamide particles by dispersion polymerization: Particle size and size distribution, *Polym. Int.* 52 (2003) 707–712.
- [26] M.S. El-Aasser, S.E. Shen, D. Sudol, Dispersion polymerization of methyl methacrylate: Mechanism of particle formation, *J. Polym. Sci. Part A: Polym. Chem.* 32 (1994) 1087–1100.
- [27] E.S. Meadows, T.J. Crowley, C.D. Immanuel, F.J. Doyle, Nonisothermal modeling and sensitivity studies for batch and semibatch emulsion polymerization of styrene, *Ind. Eng. Chem. Res.* 42 (2003) 555–567.
- [28] WHO, *Hardness in Drinking Water, Background Document for Development of WHO Guidelines for Drinking Water Quality, Health Criteria and Other Supporting Information*, vol. 2, second ed., World Health Organization, Geneva, 1996.